ACS NANOSCIENCE Au
AN OPEN ACCESS JOURNAL OF THE AMERICAN CHEMICAL SOCIETY

pubs.acs.org/nanoau Article

Direct Ink Printing of PVdF Composite Polymer Electrolytes with Aligned BN Nanosheets for Lithium-Metal Batteries

Md Golam Rasul, Meng Cheng, Yizhou Jiang, Yayue Pan, and Reza Shahbazian-Yassar*

Cite This: https://doi.org/10.1021/acsnanoscienceau.1c00056 Read Online

ACCESS | Metrics & More | Article Recommendations | Supporting Information

ABSTRACT: The use of polymer electrolytes is of great interest for lithium-metal batteries (LMBs) due to their stability with lithium metal. However, the low thermal conductivity of polymer electrolytes poses a significant barrier to minimizing the formation of local hot spots during electrochemical reactions in lithium batteries that may lead to dendritic plating of Li or thermal runaway events. Electrolyte nanocomposites with proper distribution of thermally conductive nanomaterials offer an opportunity to address this shortcoming. Utilizing a custom-designed direct ink writing (DIW) process, we show that highly aligned boron nitride (BN) nanosheets can be embedded in poly(vinylidene fluoride-hexafluoropropylene) (PVdF) polymer composite electrolytes (CPE-BN), enabling novel architectural designs for safe Li-metal batteries. It is observed that the CPE-BN electrolytes possess a 400% increase in their in-plane thermal conductivity, which enables faster heat distribution in the CPE-BN electrolyte compared to the polymer electrolytes without BN nanosheets. The CPE-BN containing symmetric lithium cell exhibits stable Li plating/stripping for over 2000 cycles without short-circuiting due to the suppression of dendritic lithium. The lithium-ion half-cells made with the CPE-BN show stable cycling performance at 1C charge−discharge rate for 250 cycles with 90% capacity retention. This reported DIW-printed PVdF composite polymer electrolyte could be used as a model for developing new architectures for other electrolytes or electrodes, thus enabling new chemistry and improved performances in energy-storage devices.

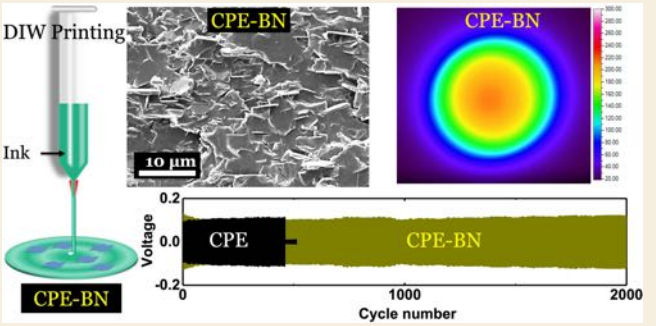

KEYWORDS: *3D printing, lithium-metal batteries, boron nitride nanosheets, heat distribution*

Downloaded via 24.148.26.224 on June 27, 2022 at 16:22:37 (UTC).
See https://pubs.acs.org/sharingguidelines for options on how to legitimately share published articles.

1. INTRODUCTION

Polymer-based electrolytes are ideal candidates for three-dimensional (3D) printing due to their desired viscoelastic properties and low melting temperature.[1−3] Among the various choices for polymer electrolytes, the poly (vinylidene fluoride-hexafluoropropylene) (PVdF) polymer has desired viscoelastic properties such as high viscosity and shear thinning behavior, enabling extrusion-based 3D printing.[1,4] PVdF is also well known for its high mechanical properties, providing structural support and superior electrochemical stability.[5] The use of PVdF-based polymer electrolytes is particularly important for lithium-metal batteries (LMBs) due to their stability with lithium metal anode resulting from a strong electron-withdrawing functional group (−C-F) in the matrix.[6,7] Despite being a promising electrolyte for 3D printing, low thermal conductivity in such polymers poses limitations in heat dissemination (local hot spots) during battery operation that may lead to battery failure and thermal runaway.[8] In addition, PVdF electrolytes show very low ionic conductivity, which can be boosted with the use of nanomaterials.[9,10]

Reinforcing PVdF polymers by incorporating thermally conductive two-dimensional (2D) materials is a promising approach to boost the thermal conductivity, mechanical strength, and electrochemical properties of PVdF polymers. To this end, BN nanosheets have shown potential as coating and additives for battery separators and electrolytes.[11−14] BN nanosheets possess impressive mechanical strength (Young's modulus 0.8 TPa, elastic modulus 510 N/m), high thermal conductivity (2000 Wm^{-1} K^{-1}), high band gap (5−6 eV), electrochemical stability, and Li^+ ion transport properties.[15] A bilayer separator was developed by sandwiching polyethylene-BN composite and PVdF to suppress dendritic lithium growth.[14] BN nanosheets have also been incorporated into gel-polymer electrolytes (GPEs) to facilitate Li^+ ion transportation. The ionic conductivity and Li^+ ion transference number of composite GPEs were significantly increased due to the Lewis acidic characteristic of BN nanosheets.[16] BN nanosheets have also been used in fabricating thermal-

Received: December 2, 2021
Revised: February 11, 2022
Accepted: February 11, 2022

© XXXX The Authors. Published by American Chemical Society

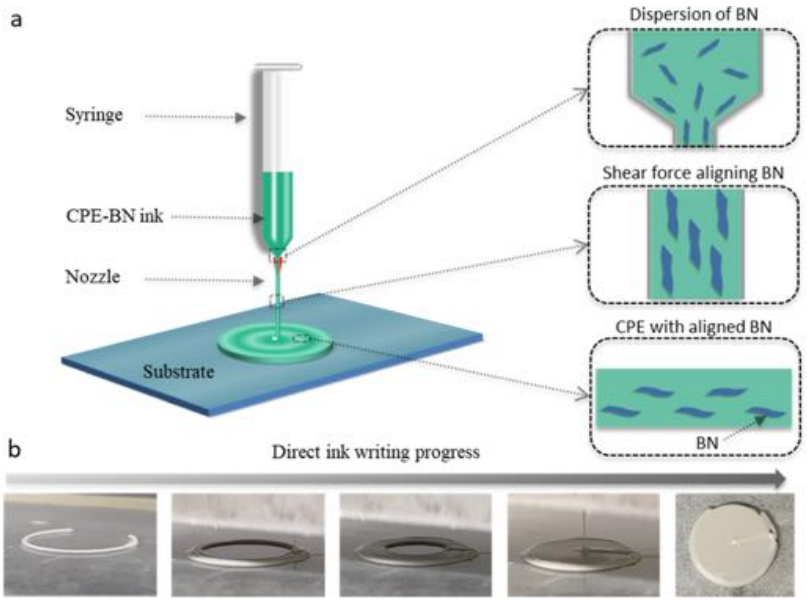

Figure 1. Illustration of the solvent-free DIW process to print highly aligned BN nanosheets in electrolyte film. (a) Schematic showing the automatically aligned BN nanosheets via shearing forces inside the extrusion nozzle. The inset schematic shows that BN nanosheets are dispersed into polymer electrolyte ink (top), BN nanosheets are aligned in the extrusion nozzle due to the shear force (middle), and printed polymer electrolytes have aligned BN nanosheets. (b) Digital images of the electrolyte film printing during the different stages of the DIW process.

regulated textiles to improve the thermal transport properties of materials for personal cooling.[17]

In previous work, we demonstrated our success in 3D printing of PVdF electrolytes reinforced with titanium dioxide nanoparticles to boost the ionic conductivity of PVdF.[18] In another study, we showed that our printing approach could be integrated with UV to chemically crosslink poly(ethylene oxide) (PEO)-based composite electrolytes reinforced with BN nanosheets.[10] However, the DIW printing of BN nanosheets incorporated PVdF polymer electrolytes without chemical crosslinking has not been reported yet. The elimination of the chemical crosslinking step improves the scalability and reduces the manufacturing cost of polymer batteries. Interestingly, several reports of PVdF-based polymer electrolytes were developed using conventional methods (i.e., solution casting and spin coating).[19−21] However, conventional methods lack control over the architectural design of microstructure constituents that are critical for achieving conformal designs of batteries or boosting their performance.[22] 3D printing technique, like the DIW process, is poised to overcome these challenges and manufacture materials with new architectures, diverse shapes, and great flexibility.[23]

Here, we show that aligned BN nanosheets are incorporated in PVdF during the direct ink writing (DIW) process without the need for chemical crosslinking (or covalent crosslinking). We demonstrate that the thermal properties, rate capability, and long-term cycling performance of LMBs can significantly be improved in PVdF + BN electrolytes in comparison to PVdF polymer electrolytes without BN nanosheets. The thermal safety of the printed electrolytes was studied by characterizing: (i) the thermal conductivity using a laser-flash technique, (ii) thermal maps using a point laser heating source, (iii) the thermal shrinkage, and (iv) cycling at high temperature (i.e., 50 °C). Moreover, the printed electrolytes were characterized for electrochemical performances: (i) galvanostatic cycling with both Li || electrolyte || Li symmetric and Li || electrolyte || lithium iron phosphate (LFP) half-cell configuration and (ii) shorting test. This study will also offer fundamental insight into the multifunctional characteristics of BN nanosheets for synthesizing thermally safe polymer electrolytes.

2. RESULTS AND DISCUSSION

Figure 1 presents a schematic diagram of the solvent-free approach of the DIW process for printing polymer electrolytes at elevated temperatures. This solvent-free approach of printing electrolyte ink is beneficial for eliminating post-processing and enables multilayered device fabrication without complexity.[18] Post-processing such as heat treatment or freeze-drying involves solvent removal from printed 3D structures, leading to structural distortion.[18] Our developed in-house temperature-controlled DIW process uses a solvent-free approach of printing electrolyte ink on substrates such as stainless steel, glass, or directly on the electrode, thus eliminating post-processing. The DIW process was developed by a robotic deposition system, including a three-axis direction stage, built-in controller, pneumatic dispenser, syringes, stainless steel blunt dispensing-nozzle, and a customized heating block.[18] The detailed procedure of printing electrolyte ink is described in the Experimental Section.

Two types of electrolyte inks were synthesized for this study: PVdF composite polymer electrolyte (CPE) and CPE with functionalized BN nanosheets (CPE-BN) inks. The CPE ink was formulated by dispersing lithium bis(trifluoromethanesulfonyl)imide (LiTFSI) salt in a mixture of PVdF polymer matrix and *N*-Propyl-*N*-methylpyrrolidinium bis(trifluoromethanesulfonyl)imide (Pyr_{13}-TFSI) ionic liquid with the help of *N*-methyl-2-pyrrolidone (NMP) solvent (Figure S2). While the electrolyte components were mixed using NMP solvent to prepare a homogeneous solution mixture, the solution mixtures were subsequently heated at 90 °C for 96 h to remove the solvent. Thermogravimetric analysis (Figure S3) indicates that the solid-like mixture (electrolyte ink) is free from NMP solvent. This electrolyte ink

https://doi.org/10.1021/acsnanoscienceau.1c00056
ACS Nanosci. Au XXXX, XXX, XXX−XXX

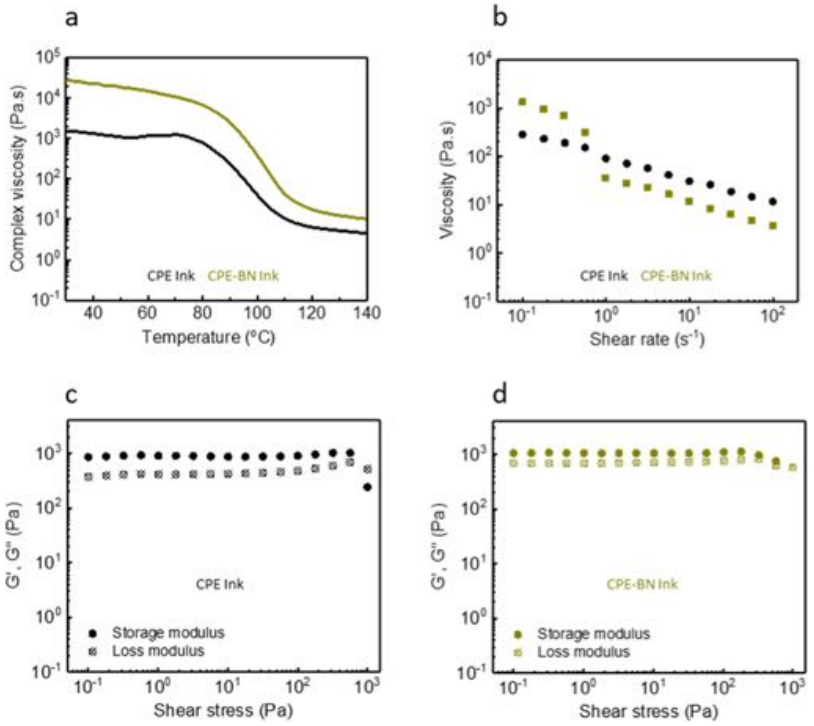

Figure 2. Rheological properties of PVdF composite polymer electrolyte inks. (a) Complex viscosity of CPE and CPE-BN inks as a function of temperature, showing 120 °C as the optimal temperature for printing. (b) Apparent viscosities of CPE and CPE-BN inks as a function of shear rate at 120 °C. (c, d) Storage modulus, G' and loss modulus, G'' as a function of shear stress for CPE and CPE-BN inks.

was later used to print the electrolytes (CPE and CPE-BN) using DIW techniques at 120 °C. Pyr_{13}-TFSI ionic liquid was added into the PVdF matrix to steer the rheological properties and improve the safety and Li^+ ion conductivity of the electrolyte inks.[24] The Pyr_{13}-TFSI ionic liquid is also well known for dissolving the LiTFSI lithium salts, facilitating Li^+ ion transportation through the electrolyte ink.[24]

CPE-BN inks were synthesized using 0.5 wt % silane-functionalized BN nanosheets. The lack of functional molecular presence on nonfunctionalized BN (pristine BN) nanosheets surface leads to weak molecular interaction at the PVdF-BN interface, resulting in inferior mechanical, thermal, and electrochemical properties of the electrolytes.[15] Therefore, silane-functionalized BN nanosheets were utilized to formulate CPE-BN electrolytes. Silane-functional groups were chosen to functionalize BN nanosheets (characterization of silane-functionalized BN nanosheets are provided in Figure S4, Supporting Information) since it has both nonpolar alkyl molecules (−R), which are compatible with the nonpolar molecule ($-CH_2-$) of PVdF and polar molecules (O_2), which facilitate in H-bond formation with polar part of PVdF (−F). In addition, the electronegative molecules can also attach with $TFSI^-$ anions, thus releasing free Li^+ ions and increase ionic conductivity.[25] As a result, the mechanical and electrochemical properties of CPE reinforced with silane-functionalized BN are superior compared to the pristine BN nanosheets, as evidenced from Figures S5, S6, and Table S1. The silane coupling agent also reduces thermal interfacial resistance at the polymer-BN interface, resulting in an enhanced thermal conductivity of the composites, as reported in our previous publication.[26] To find out the optimum amount of functionalized BN nanosheets loading, the ionic conductivity of CPE with 0 to 1.0 wt % functionalized BN nanosheets were measured. As evidenced from experimental results (Figure S7, Supporting Information), the optimum 0.5 wt % functionalized BN nanosheets result in the maximum ionic conductivity (6.74×10^{-4} S/cm). The detailed procedure for synthesizing the electrolyte inks is provided in the Experimental Section (Supporting Information).

The rheological properties of inks, including their complex-apparent viscosities and storage-loss moduli, are important parameters that are tailored to design an ink for extrusion-based printing.[2] The complex viscosities of CPE and CPE-BN inks were measured by heating the samples from 30 to 140 °C at a heating rate of 3 °C per minute and plotted in Figure 2a. As demonstrated, the complex viscosities of both inks were decreased slowly with the increasing temperature up to 80 °C. However, the viscosity decreased rapidly in the temperature region from 80 to 110 °C, indicating liquid-like behavior at 120 °C. Therefore, the printing temperature for both CPE and CPE-BN inks was set at 120 °C, providing an ideal condition for the continuous filament formation without clogging during electrolyte printing. Further, the apparent viscosities of both inks show shear thinning behavior at 120 °C, enabling printing complex 3D architecture on the substrate (Figure 2b).[27] Compared to CPE, the high viscosity of CPE-BN inks indicates the physisorption of PVdF molecular chains onto the BN nanosheets surfaces. At a high shear rate, i.e., 0.3 s^{-1}, the viscosity decreased, which can be explained by the reduction of entanglement density. Figure 2c,d shows the storage and loss modulus as a function of shear stress at 120 °C. Both CPE and CPE-BN inks storage modulus are higher than loss modulus in the 0.1−100 Pa shear stress region, indicating solid-like behavior, suitable for maintaining the 3D structure after extrusion. On the other hand, loss modulus is higher than the storage modulus at high shear stress (i.e., 100−1000 Pa), indicating liquid-like behavior, which is beneficial to ink flow through the nozzle during printing. Considering the

https://doi.org/10.1021/acsnanoscienceau.1c00056
ACS Nanosci. Au XXXX, XXX, XXX−XXX

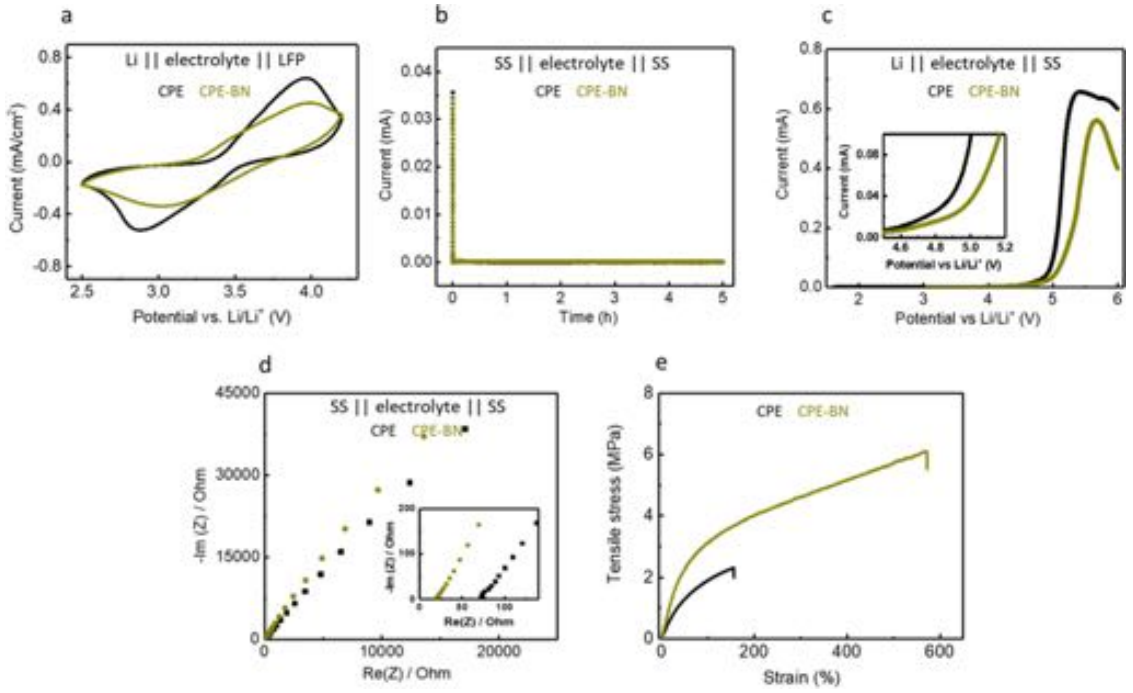

Figure 3. Electrochemical and mechanical characterization of the synthesized CPE and CPE-BN electrolytes. (a) Cyclic voltammograms (CV) of the Li || electrolyte || LFP cells with a scan rate of 1.0 mV s^{-1}, showing symmetric peaks. (b) Direct current polarization (DCP) tests of the SS || electrolyte || SS cells with a polarization voltage of 0.5 V to measure the electrical conductivity of the electrolytes. (c) Linear sweep voltammetry (LSV) of the Li || electrolyte || SS cells showing electrochemical stability window in the potential range of 3−6 V with a scan rate of 1.0 mV s^{-1}. (d) Impedance spectroscopy results of the symmetric SS || electrolyte || SS cells with CPE and CPE-BN electrolytes. (e) Stress−strain test results of the CPE and CPE-BN.

rheological properties of both inks, the printing parameters were set to extrude through the nozzle, and electrolyte films were printed onto different substrates, including stainless steel (SS), glass, and electrode materials. The printed electrolyte films are self-standing and flexible, as shown in Figure S8, which are necessary for developing energy storage devices. Their surface morphology of the printed electrolytes shows that the pore sizes of CPE and CPE-BN can accommodate all Pyr_{13}^+, $TFSI^-$, and Li^+ ions because of their much larger size compared to the ion sizes (Figure S9).

2.1. Characterization of PVdF Composite Polymer Electrolyte

The synthesized polymer electrolytes were characterized to ensure their electrochemical suitability in energy storage devices. Cyclic voltammetry (CV) test was performed to observe the intercalation and deintercalation in the LFP cathode. As demonstrated in Figure 3a, cells containing both CPE and CPE-BN electrolytes show symmetric redox (oxidation at 3.95 V and reduction at 2.87 V) peaks, indicating reversibility of Li^+ ion intercalation and deintercalation with the LFP lattice structure. This points to the successful Li^+ ion shuttling through the synthesized polymer electrolytes (Figure 3a). There were no additional peaks observed, confirming the absence of side reactions. The electrolytes were further characterized by a direct current (DC) polarization test using a SS || electrolyte || SS symmetric cell. These cells were tested with a polarization voltage of 0.5 V to measure the electrical conductivity of the printed electrolytes. The calculated electrical conductivity of CPE and CPE-BN is 5.3×10^{-7} and 4.1×10^{-7} S/cm, respectively, confirming the electrical nonconductivity of the electrolytes (Figure 3b). Therefore, the printed electrolytes can be used for safe Li^+ ion transportation without any internal short circuit.[28]

The electrochemical stabilities of CPE and CPE-BN electrolytes were evaluated by measuring linear sweep voltammetry (LSV), with a scan rate of 1.0 mV s^{-1} (Figure 3c). During the scan, an oxidative current starts to increase at 4.8 V (vs Li/Li^+) for the CPE electrolyte (inset of Figure 3c), indicating the onset of the oxidative decomposition of the electrolytes.[29] In sharp contrast, CPE-BN is stable up to 5.0 V (vs Li/Li^+), indicating the decomposition voltage of CPE-BN is higher than CPE. The excellent electrochemical stability of CPE-BN is likely originated from the solid dipole−dipole interaction between the functionalized BN and electrolyte components such as LiTFSI and PVdF. PVdF polymer has polar molecules that could interact with polar molecules of functionalized BN, increasing the electron transition energy level of PVdF decomposition and increasing the electrochemical stability of the electrolytes.[30,31] Such dipole−dipole interaction could also lead to forming a complexation between $TFSI^-$ anion and functionalized BN, resulting in the retardation of decomposition of $TFSI^-$ anions and increased electrochemical stability of the electrolyte.[30] As a result of having higher electrochemical stability, CPE-BN electrolytes could have an electrochemical operation with a broader voltage window, enabling its use with high energy density cathode materials compared to the CPE.[32]

The benefits of BN nanosheets addition were further investigated by studying the electrochemical impedance spectroscopy (EIS) and stress−strain test results of the electrolytes. The calculated ionic conductivity is 1.0×10^{-4} S/cm for CPE and 6.74×10^{-4} S/cm for CPE-BN at room temperature. The ionic conductivity of the CPE-BN is 6 times

https://doi.org/10.1021/acsnanoscienceau.1c00056
ACS Nanosci. Au XXXX, XXX, XXX−XXX

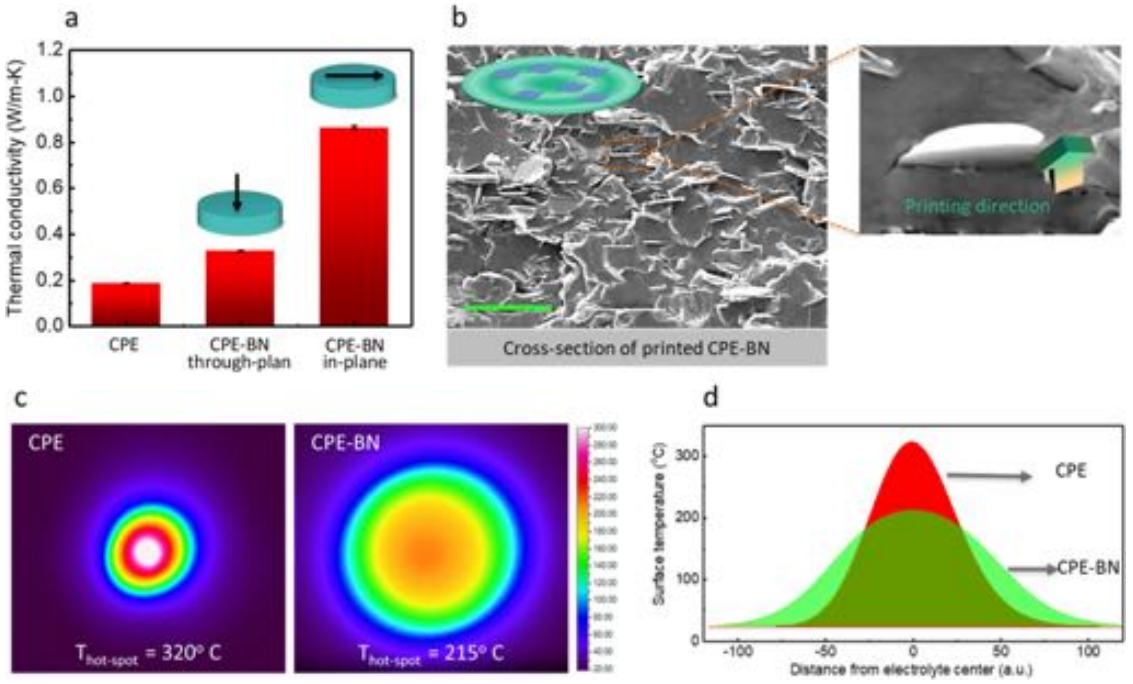

Figure 4. Thermal evaluation of the CPE and CPE-BN electrolytes. (a) Thermal conductivity of electrolytes. (b) Cross-sectional SEM images of CPE-BN electrolytes, showing highly aligned BN nanosheets along the printing direction (the inset shows a schematic diagram of the CPE-BN with aligned BN nanosheets). Scale bar 10 μm. (c) IR images of the temperature distribution of the CPE and CPE-BN electrolytes at laser source power of 100 μW. (d) Surface temperature profile of the electrolytes shown in (c).

higher than the CPE, which is above the benchmark value for battery electrolytes (Figure 3d).[33] The increment of ionic conductivity could likely be attributed to the functional silane groups and Lewis acid−base characteristics of BN nanosheets.[16,25] The functional silane groups of BN contain electronegative molecules (−O), which could attract the $TFSI^-$ anions of LiTFSI salts and release free Li^+ ions (Figure S10).[25] In addition, the B atoms of BN can interact with other Lewis bases due to their own Lewis acidic characteristics.[16] Such features could trap the $TFSI^-$ anions and release the Li^+ ions, resulting in an increase in both ionic conductivity and transference (t_{Li+}) values (Figures S11, S12, and Table S2, Supporting Information) of CPE-BN (t_{Li+} is 0.19 for CPE-BN vs 0.11 for CPE). This could further facilitate suppressing dendritic Li formation (the results are shown in the proceeding sections).[34]

The mechanical reinforcement of BN nanosheets in PVdF polymer electrolytes was analyzed by stress−strain test result (Figure 3e), demonstrating the chain entanglement and molecular interactions between BN nanosheets and PVdF matrix. The calculated Young's modulus and strength of the CPE-BN (5.92 and 6.12 MPa) are 98 and 168% higher than CPE (3.34 and 2.28 MPa). This increase in modulus and strength was achieved without reducing its ductility, indicating 10 times higher toughness of the CPE-BN (24.6 MJ/m^3) than the CPE (2.4 MJ/m^3). The increase in mechanical strength, modulus, and toughness could be attributed to the H-bond formation between electronegative fluorine atoms of PVDF matrix and hydrogen atoms of functionalized BN molecules (Figure S13).[35]

2.2. Thermal Safety

The thermal safety performance of the printed PVdF composite polymer electrolyte is characterized by evaluating the thermal conductivity, thermal distribution, and heat shrinkage properties. Heat could be generated during cycling operation of LMBs for the following instances: (i) intrinsic internal resistance of the battery, leading to heat generation due to charge/discharge process, (ii) existence of an external stimulus such as ambient temperature rise or mechanical impact, and (iii) occurrence of an internal stimulus such as short circuit, overcharge, or applied high current rates (i.e., high C-rates).[36−38] The thermal conductivity of the printed electrolyte was measured using the laser-flash technique, and the results are shown in Figure 4a. The measured thermal conductivities are 0.2 Wm^{-1} K^{-1} for CPE and 0.3 and 0.85 Wm^{-1} K^{-1} for the through-plane and in-plane direction of the CPE-BN, respectively. Typically, the electrolyte has low thermal conductivity and is sandwiched between two electrodes, thus blocking the heat generated within the battery in both in-plane and through-plane directions. In sharp contrast, the BN nanosheets of the CPE-BN are highly aligned, as shown in the cross-sectional microstructure in Figure 4b, resulting in a very high thermal conductivity along the in-plane direction of the composite films. Therefore, the heat generated within the battery could easily be distributed in both in-plane (radial) and through-plane (axial) directions.

To demonstrate the effect of enhanced thermal conductivity, electrolyte films were heated separately using a point laser heating source to heat the films locally, and the distribution of the surface temperature was recorded using a micro thermal imaging microscope (Figure 4c,d). Because of the local heating, hot spots are formed on the sample surfaces. The highest hot-spot temperature was 320 °C on the CPE surface (Figure 4c), suggesting that the generated heat cannot be disseminated through the samples due to low thermal conductivity. In contrast, the hot-spot temperature of CPE-BN films shows 215 °C, which is 33% lower than CPE. As shown in Figure 4d, the heat generated by the laser was

https://doi.org/10.1021/acsnanoscienceau.1c00056
ACS Nanosci. Au XXXX, XXX, XXX−XXX

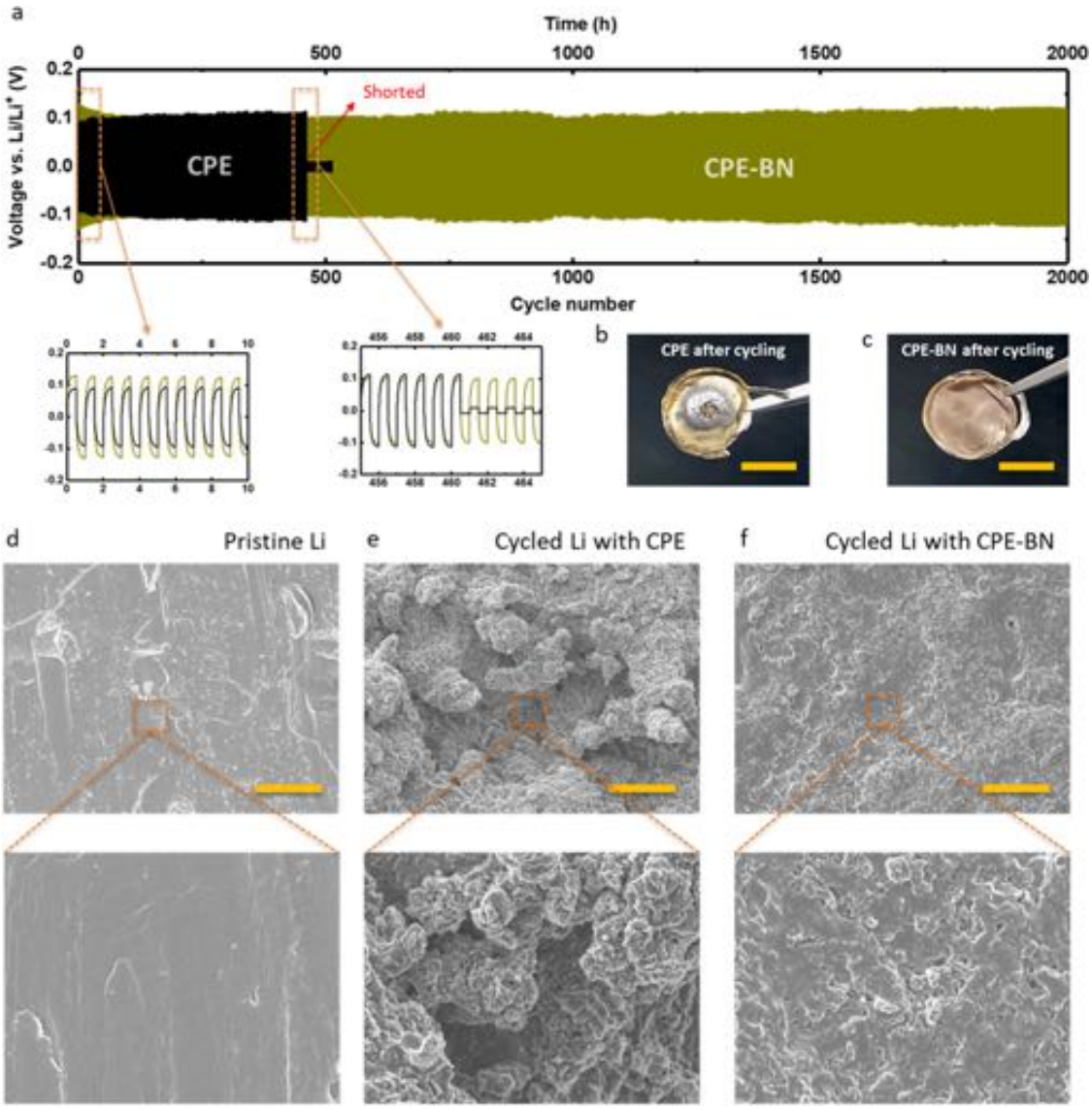

Figure 5. Cycling stability of Li || electrolyte || Li symmetric cells with CPE and CPE-BN. (a) Galvanostatic cycling of the Li || electrolyte || Li symmetric cell with a constant current density of 0.1 mA cm^{-2} for a plating/stripping time of T_c = 0.5 h. Representative cycle numbers 1−10 and 455−465 cycling tests were carried out at current densities of 0.1 mA cm^{-2}. (b, c) Optical image of the CPE and CPE-BN after being cycled in a Li || electrolyte || Li symmetric cell. d. SEM images of pristine Li-metal surfaces (before cycling). SEM images of the Li-metal surface of the Li || electrolyte || Li symmetric cell after being cycled, where the electrolyte is CPE (e) and CPE-BN (f). All scale bars for (d)−(f) are 50 μm, and that for (b) and (c) are 10 mm.

transported throughout the sample surfaces, indicating minimized hot-spot formation for CPE-BN. The improved thermal distribution capability of the CPE-BN compared to CPE could attribute to the following results of (i) increased thermal conductivity and (ii) the lower heat absorption of CPE-BN composites, as reported in other literature.[26]

The thermal safety of the printed PVdF composite polymer electrolytes was further tested by the heat shrinkage and shorting test. Figure S14 demonstrates the heat shrinkage test of the CPE and CPE-BN, showing the thermal stability at high-temperature battery operation. Thermal shrinkage of the printed electrolytes was evaluated by heat treatment at different temperatures for 20 min and demonstrated in Figure S14. At elevated temperatures (e.g., 250 °C), the CPE-BN film retained its shape, while the shape of the CPE film size was reduced by 20%. When the hot-plate temperature was increased to 300 °C, the CPE-BN film was reduced by just 3.3% compared to CPE by 33.3%. The results indicate that the CPE-BN film can disseminate thermal stress due to its high thermal conductivity, thus enduring high temperature and delivering better thermal stability than the CPE.[39] Thermogravimetric analysis of the printed electrolytes shows improved thermal stability of the CPE-BN electrolytes compared to CPE (Figure S15). The enhanced thermal stability of the CPE-BN is beneficial for minimizing the short circuit events at high temperatures.

2.3. Electrochemical Performance

To demonstrate the long-term cyclability and electrochemical stability against the Li-metal surface, the galvanostatic cycling test is carried out in a Li || electrolyte || Li symmetric cell with a constant areal current density of 0.1 mA cm^{-2} for a plating/stripping time of T_c = 0.5 h. Figure 5 shows the overpotentials vs time (and cycle number) plot for the Li || electrolyte || Li

https://doi.org/10.1021/acsnanoscienceau.1c00056
ACS Nanosci. Au XXXX, XXX, XXX−XXX

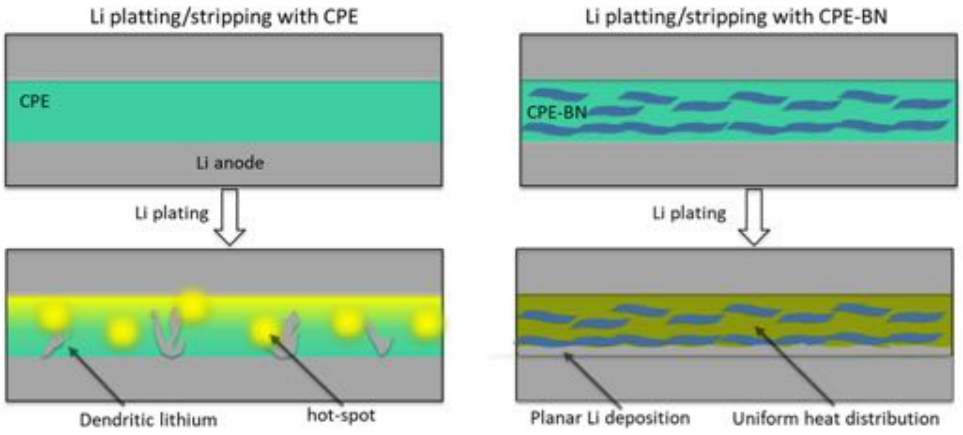

Figure 6. A schematic diagram of the printed PVdF composite polymer electrolytes (CPE and CPE-BN). Aligned BN nanosheets facilitate the heat distribution homogeneously and mechanically suppress the dendritic Li growth during Li plating/stripping.

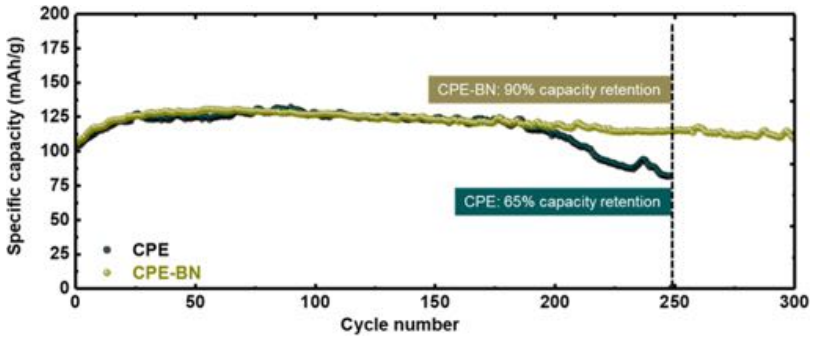

Figure 7. Discharge capacities of the Li || electrolyte || LFP cells with CPE and CPE-BN electrolytes cycled at 1C rate (140 mA g^{-1}) at 25 °C.

symmetric cell setup with CPE and CPE-BN electrolytes. The overpotential for the battery with the CPE was gradually increased from 0.09 to 0.11 V during the first 100 cycles and stabilized till 461 cycles. After 461 cycles, the cell employed with the CPE short-circuited. The sharp decrease can confirm voltage hysteresis with cycle time (461 h).[40] This poor cycling performance could be ascribed to the dendritic lithium formation and the undesirable reactions between the Li metal and the electrolyte during cycling.[41] This was further evidenced by the SEM images of the cycled Li surfaces obtained by disassembling the cells after the cycling test (Figure 5d,e). The Li surface cycled with the CPE shows a rough morphology, indicating uncontrolled dendritic lithium formation.

In contrast, the initial plating/stripping overpotentials (0.09 V for CPE and 0.13 V for CPE-BN) indicate that the CPE-BN has higher polarization than the CPE. This suggests that BN induces slight resistance to the battery. During Li^+ ion shuttling through the electrolytes, BN could act as Li^+ ion diffusion barrier due to its electronic interaction and redistribution inside the materials, leading the diffusion barrier for BN to as high as 6.75 eV.[42] This Li^+ ion diffusion barrier largely depends on the structure, assembly, defect pattern, bond length, and proximity effect of BN nanosheets, indicating that it is very hard for Li^+ ion to diffuse through them.[42] Therefore, the slightly higher polarization voltage could be attributed to the energy barriers that Li^+ ions need to overcome. The polarization voltage of the CPE-BN was reduced to 0.09 V after 100 cycles and continued stable cycling for over 2000 cycles, indicating long-term stability of the electrolyte against Li metal. Such long-term cycling stability of CPE-BN could be attributed to several possible reasons (Figure 6). First, the mechanical modulus and strengths of the CPE-BN are 2 times higher than the CPE, leading to increased resistance in suppressing dendritic lithium formation.[43] Besides, the increased toughness of the CPE-BN likely accommodates the volume changes that might occur during cycling, leading to stable electrolyte structure during long-term cycling. Second, the BN nanosheets are aligned in the CPE-BN, which possess a much higher modulus (Young's modulus 0.8 TPa, elastic modulus 510 N/m) and strength (fracture strength 26.3 GPa), could further suppress the dendritic lithium growth, resulting in planner deposition of Li.[44,45] Third, the increased thermal conductivity of the CPE-BN facilitates distributing heat homogeneously, resulting in uniform heat distribution and regulated lithium deposition.[46] This was further evidenced by the SEM images of the cycled Li surfaces obtained by disassembling the cells after the cycling test, showing smooth Li surfaces (Figure 5f). Because of the synergistic effect of the highly aligned BN nanosheets, a uniform lithium deposition could be achieved, and dendritic lithium formation could be avoided for batteries with CPE-BN electrolytes. There was a slightly lower overpotential of the CPE-BN, indicating more accessible Li^+ transportation than CPE, attributed to the higher ionic conductivity and increased Li transference number (Figures S7, 11, 12, and Table S2; Supporting Information).[16]

The dendritic lithium suppression was further supported by a shorting test conducted in a Li || electrolyte || Li symmetric cell by charging it with a constant current density of 0.3 mA cm^{-2}. As demonstrated in Figure S16, the CPE was shorted after 32 h of Li deposition, while CPE-BN was shorted after 68 h, indicating a more substantial barrier to suppress dendritic Li.

https://doi.org/10.1021/acsnanoscienceau.1c00056
ACS Nanosci. Au XXXX, XXX, XXX−XXX

The corresponding microscopy of the lithium surface obtained from the dissembled cell reveals that the CPE-employed lithium surface is much rougher as compared to the CPE-BN-employed lithium surface (Figure S16).

The CPE and CPE-BN electrolytes were assembled in Li || electrolyte || LFP cells. Their cycling performances were tested at room temperature (i.e., 25 °C) and an elevated temperature (i.e., 50 °C). The room-temperature cycling performances of cells containing the CPE and CPE-BN at 1C rate of charge−discharge rate are shown in Figure 7. The Li || CPE || LFP cell delivers a steady discharge capacity of 132 mAh g^{-1} up to 130 cycles, after which the discharge capacity starts to degrade. The capacity retention of the Li || CPE || LFP cell after 250 cycles shows 65%. In sharp contrast, the Li || CPE-BN || LFP cell delivers a steady discharge capacity, indicating capacity retention of 90% after 250 cycles. This shows that the CPE-BN has better cycling stability and capacity retention than the CPE, which could be attributed due to the suppression of dendritic Li formation and electrochemical stability of the electrolyte/Li interface. While this work provides adequate insight into the role of BN nanosheets and their alignment in suppressing the dendritic lithium growth, it would be interesting to investigate the electrochemistry of full-cell battery performance in future endeavors. In addition, a dense layer was found at the electrode/electrolyte interface, which is possibly formed during the DIW of electrolytes on the electrode substrate directly (Figure S17). During the extrusion of the inks, the melted PVdF matrix could bond with the electrode strongly because of the common binders, i.e., PVdF in both the electrode and electrolytes. Such a dense layer could provide close contact, attributing to the structural integrity of the electrolyte and electrode interface during long-term cycling performance.[18]

The electrolytes were further tested in an Li || electrolyte || LFP cell at an elevated temperature (i.e., 50 °C), with a 2C charge−discharge rate. The cycling results (Figure S18) showed no significant capacity degradation for cells with CPE-BN, indicating stable electrolytes even under a harsh electrochemical environment than CPE.[32] The capacity retention of cells shows 90% for the CPE-BN and 68% for CPE, respectively. This points that the CPE-BN is stable under harsh electrochemical environments like 2C rate charge-discharge operation, which requires long-term exposure to electrochemical processes and high temperature.[47,48] The half-cell cycling performance of cells with our DIW-printed electrolytes performed better when compared with the conventional method-prepared PVdF-based composite electrolytes (Table S4). This improved performance could be ascribed to the highly aligned BN nanosheets assembly into the composite electrolyte matrix. As demonstrated (Figure S19), the randomly oriented BN nanosheets could not provide a sufficient barrier to suppress the dendritic lithium growth. In contrast, aligned BN nanosheets can regulate the Li-ion deposition to planner morphology, resulting in improved cycle performances.

Figure 8 shows the rate capability test of Li || CPE || LFP and Li || CPE-BN || LFP cells at 50 °C by increasing the C-rate from 0.1 to 2.0 C. The initial discharge capacities of both cells (150 mAh g^{-1} for CPE and 156 mAh g^{-1} for CPE-BN) are close to the theoretical capacity values of LFP (165 mAh g^{-1}). With the increasing C-rate from 0.1 to 2.0, the discharge capacity decreases, and 117 mAh g^{-1} was attained for CPE and 120 mAh g^{-1} for CPE-BN at 2C rate. Furthermore, the

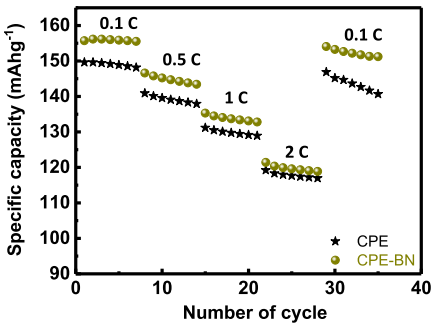

Figure 8. Rate capability performance of the CPE and CPE-BN electrolytes at 50 °C for a current density of 16.5 (0.1C), 82.5 (0.5C), 165 (1C), and 330 (2C) mA g^{-1}, respectively, in the Li || electrolyte || LFP cell.

discharge capacity recovers to the initial values (143 mAh g^{-1} for CPE and 152 mAh g^{-1} for CPE-BN) when the C-rate is decreased from 2.0 to 0.1C. CPE-BN recovers its initial discharge capacity, indicating improved reversible capacity recovery behavior compared to CPE.

Overall, PVdF composite polymer electrolytes with aligned and functionalized BN nanosheets are printed using a solvent-free DIW technique at an elevated temperature. The CPE-BN electrolytes exhibit high thermal conductivity owing to the distribution of aligned BN nanosheets, resulting in enhanced thermal distribution and reduced hot-spot formation. Coupled with improved thermal properties, the printed electrolytes could cycle for more than 2000 cycles without short-circuiting and electrochemical degradation even under a harsh electrochemical environment. This work provides new opportunities to develop the next-generation LMBs with new architectures and improved performances.

3. CONCLUSIONS

In summary, we report a direct printing of highly aligned BN nanosheets incorporated within PVdF composite polymer electrolyte inks in a solvent-free DIW approach. This CPE-BN is mechanically strong, electrochemically stable, and thermally safe. LMBs using this printed electrolyte are durable for over 2000 cycles without short-circuiting in symmetric Li || CPE-BN || Li cell and demonstrate high C-rate cycling performance in Li || CPE-BN || LFP configuration. The discharge capacity was maintained at 90% for over 100 cycles at 2C-rate and 250 cycles at 1C-rate for LMBs with the CPE-BN electrolytes. Such high-performance could be achieved because of the highly aligned BN nanosheets structures and a dense layer formed at the interface of electrode/electrolyte induced by the printing process. Thus, the DIW-printed PVdF composite polymer electrolytes represent a promising route to develop LMBs that are thermally safe, electrochemically stable, and capable of high C-rates for long-term cycling performance.

■ ASSOCIATED CONTENT

Supporting Information

The Supporting Information is available free of charge at https://pubs.acs.org/doi/10.1021/acsnanoscienceau.1c00056.

Additional information on the experimental details (functionalization of BN nanosheets, electrolyte ink synthesis, LFP cathode preparation, ink printing to fabricate CPE and CPE-BN using DIW method), characterization techniques (microscopy, mechanical,

https://doi.org/10.1021/acsnanoscienceau.1c00056
ACS Nanosci. Au XXXX, XXX, XXX−XXX

thermal testing, electrochemical characterization), and characterization results (microstructural characterization of BN nanosheets, ink synthesis, thermogravimetric analysis of ink-solution mixture, silane-functionalization characterization, stress−strain test results, optical images of stress−strain test result, EIS characterization, digital images of electrolyte films, SEM images of electrolytes, illustration of $TFSI^-$ anion trapping, transference calculation, schematic diagram of H-bond formation, thermal shrinkage test results, thermal stability of inks, electrochemical shorting test results, cross-sectional SEM images, cycling performance at higher C-rate at 50 °C, battery performance comparison, and schematic diagram of thermal safety and dendrite suppression comparison) (PDF)

AUTHOR INFORMATION

Corresponding Author

Reza Shahbazian-Yassar − *Mechanical and Industrial Engineering Department, University of Illinois at Chicago, Chicago, Illinois 60607, United States;* orcid.org/0000-0002-7744-4780; Email: rsyassar@uic.edu

Authors

Md Golam Rasul − *Mechanical and Industrial Engineering Department, University of Illinois at Chicago, Chicago, Illinois 60607, United States*

Meng Cheng − *Mechanical and Industrial Engineering Department, University of Illinois at Chicago, Chicago, Illinois 60607, United States*

Yizhou Jiang − *Mechanical and Industrial Engineering Department, University of Illinois at Chicago, Chicago, Illinois 60607, United States*

Yayue Pan − *Mechanical and Industrial Engineering Department, University of Illinois at Chicago, Chicago, Illinois 60607, United States;* orcid.org/0000-0003-0797-1697

Complete contact information is available at: https://pubs.acs.org/10.1021/acsnanoscienceau.1c00056

Notes

The authors declare no competing financial interest.

ACKNOWLEDGMENTS

This project is financially supported by National Science Foundation Award No. CBET-1805938. The authors also acknowledge the Battery Technology Laboratory of the College of Engineering at the University of Illinois at Chicago (UIC). Parts of the characterization works were carried out at the Materials Characterization and Imaging Facility (MatCI), which receives support from the MRSEC Program (NSF DMR-1720139) of the Materials Research Center at Northwestern University. The thermal conductivity of samples was measured at the NETZSCH Instruments Applications Laboratory, Burlington, MA.

REFERENCES

(1) Zhu, C.; Han, T. Y. J.; Duoss, E. B.; Golobic, A. M.; Kuntz, J. D.; Spadaccini, C. M.; Worsley, M. A. Highly Compressible 3D Periodic Graphene Aerogel Microlattices. *Nat. Commun.* **2015**, *6*, No. 6962.

(2) Lewis, J. A.; Gratson, G. M. Direct Writing in Three Dimensions. *Mater. Today* **2004**, *7*, 32−39.

(3) Hon, K. K. B.; Li, L.; Hutchings, I. M. Direct Writing Technology-Advances and Developments. *CIRP Ann.* **2008**, *57*, 601−620.

(4) Li, Y.; Gao, T.; Yang, Z.; Chen, C.; Luo, W.; Song, J.; Hitz, E.; Jia, C.; Zhou, Y.; Liu, B.; Yang, B.; Hu, L. 3D-Printed, All-in-One Evaporator for High-Efficiency Solar Steam Generation under 1 Sun Illumination. *Adv. Mater.* **2017**, *29*, No. 1700981.

(5) Du Pasquier, A.; Warren, P. C.; Culver, D.; Gozdz, A. S.; Amatucci, G. G.; Tarascon, J. M. Plastic PVDF-HFP Electrolyte Laminates Prepared by a Phase-Inversion Process. *Solid State Ionics* **2000**, *135*, 249−257.

(6) Xie, L.; Huang, X.; Yang, K.; Li, S.; Jiang, P. "Grafting to" Route to PVDF-HFP-GMA/BaTiO3 Nanocomposites with High Dielectric Constant and High Thermal Conductivity for Energy Storage and Thermal Management Applications. *J. Mater. Chem. A* **2014**, *2*, 5244.

(7) Liu, F.; Hashim, N. A.; Liu, Y.; Abed, M. R. M.; Li, K. Progress in the Production and Modification of PVDF Membranes. *J. Memb. Sci.* **2011**, *375*, 1−27.

(8) Choudhury, S.; Stalin, S.; Vu, D.; Warren, A.; Deng, Y.; Biswal, P.; Archer, L. A. Solid-State Polymer Electrolytes for High-Performance Lithium Metal Batteries. *Nat. Commun.* **2019**, *10*, No. 4398.

(9) Wang, F.; Li, L.; Yang, X.; You, J.; Xu, Y.; Wang, H.; Ma, Y.; Gao, G. Influence of Additives in a PVDF-Based Solid Polymer Electrolyte on Conductivity and Li-Ion Battery Performance. *Sustainable Energy Fuels* **2018**, *2*, 492−498.

(10) Cheng, M.; Ramasubramanian, A.; Rasul, M. G.; Jiang, Y.; Yuan, Y.; Foroozan, T.; Deivanayagam, R.; Tamadoni Saray, M.; Rojaee, R.; Song, B.; Yurkiv, V. R.; Pan, Y.; Mashayek, F.; Shahbazian-Yassar, R. Direct Ink Writing of Polymer Composite Electrolytes with Enhanced Thermal Conductivities. *Adv. Funct. Mater.* **2021**, *31*, No. 2006683.

(11) Luo, W.; Zhou, L.; Fu, K.; Yang, Z.; Wan, J.; Manno, M.; Yao, Y.; Zhu, H.; Yang, B.; Hu, L. A Thermally Conductive Separator for Stable Li Metal Anodes. *Nano Lett.* **2015**, *15*, 6149−6154.

(12) Li, H.; Tay, R. Y.; Tsang, S. H.; Liu, W.; Teo, E. H. T. Reduced Graphene Oxide/Boron Nitride Composite Film as a Novel Binder-Free Anode for Lithium Ion Batteries with Enhanced Performances. *Electrochim. Acta* **2015**, *166*, 197−205.

(13) Tutgun, M. S.; Sinirlioglu, D.; Celik, S. U.; Bozkurt, A. Effect of Hexagonal Boron Nitride on Poly(Vinyl Phosphonic Acid) Composite Polymer Electrolytes for Fuel Cells. *Polym. Sci. Ser. A* **2016**, *58*, 810−817.

(14) Waqas, M.; Ali, S.; Lv, W.; Chen, D.; Boateng, B.; He, W. High-Performance PE-BN/PVDF-HFP Bilayer Separator for Lithium-Ion Batteries. *Adv. Mater. Interfaces* **2019**, *6*, No. 1801330.

(15) Rasul, M. G.; Kiziltas, A.; Arfaei, B.; Shahbazian-Yassar, R. 2D Boron Nitride Nanosheets for Polymer Composite Materials. *npj 2D Mater. Appl.* **2021**, *5*, No. 56.

(16) Shim, J.; Kim, H. J.; Kim, B. G.; Kim, Y. S.; Kim, D. G.; Lee, J. C. 2D Boron Nitride Nanoflakes as a Multifunctional Additive in Gel Polymer Electrolytes for Safe, Long Cycle Life and High Rate Lithium Metal Batteries. *Energy Environ. Sci.* **2017**, *10*, 1911−1916.

(17) Gao, T.; Yang, Z.; Chen, C.; Li, Y.; Fu, K.; Dai, J.; Hitz, E. M.; Xie, H.; Liu, B.; Song, J.; Yang, B.; Hu, L. Three-Dimensional Printed Thermal Regulation Textiles. *ACS Nano* **2017**, *11*, 11513−11520.

(18) Cheng, M.; Deivanayagam, R.; Foroozan, T.; Rojaee, R.; Shokuhfar, T.; Lu, J.; Yao, W.; Shahbazian-Yassar, R.; Song, B.; Pan, Y.; Jiang, Y.; Yuan, Y.; Huang, Z. Elevated-Temperature 3D Printing of Hybrid Solid-State Electrolyte for Li-Ion Batteries. *Adv. Mater.* **2018**, *30*, No. 1800615.

(19) Chen, H.; Xu, P.; Chen, L.; Li, X.; Ding, Y. Enhanced Ion Transport in PVDF-HFP Gel Polymer Electrolyte Containing PDA@BN for Lithium Ion Batteries. *Mater. Lett.* **2020**, *277*, No. 128391.

(20) Bian, X.; Liang, J.; Tang, X.; Li, R.; Kang, L.; Su, A.; Su, X.; Wei, Y. A Boron Nitride-Polyvinylidene Fluoride-Co-Hexafluoropropylene Composite Gel Polymer Electrolyte for Lithium Metal Batteries. *J. Alloys Compd.* **2019**, *803*, 1075−1081.

(21) Zhang, Z.; Antonio, R. G.; Choy, K. L. Boron Nitride Enhanced Polymer/Salt Hybrid Electrolytes for All-Solid-State Lithium Ion Batteries. *J. Power Sources* **2019**, *435*, No. 226736.
(22) Wei, T. S.; Ahn, B. Y.; Grotto, J.; Lewis, J. A. 3D Printing of Customized Li-Ion Batteries with Thick Electrodes. *Adv. Mater.* **2018**, *30*, No. 1703027.
(23) Cheng, M.; Deivanayagam, R.; Shahbazian-Yassar, R. 3D Printing of Electrochemical Energy Storage Devices: A Review of Printing Techniques and Electrode/Electrolyte Architectures. *Batteries Supercaps* **2020**, *3*, 130−146.
(24) Deivanayagam, R.; Cheng, M.; Wang, M.; Vasudevan, V.; Foroozan, T.; Medhekar, N. V.; Shahbazian-Yassar, R. Composite Polymer Electrolyte for Highly Cyclable Room-Temperature Solid-State Magnesium Batteries. *ACS Appl. Energy Mater.* **2019**, *2*, 7980−7990.
(25) Rojaee, R.; Shahbazian-Yassar, R. Two-Dimensional Materials to Address the Lithium Battery Challenges. *ACS Nano* **2020**, *14*, 2628−2658.
(26) Rasul, M. G.; Kiziltas, A.; Bin Hoque, M. S.; Banik, A.; Hopkins, P. E.; Tan, K.-T.; Arfaei, B.; Shahbazian-Yassar, R. Improvement of the Thermal Conductivity and Tribological Properties of Polyethylene by Incorporating Functionalized Boron Nitride Nanosheets. *Tribol. Int.* **2022**, *165*, No. 107277.
(27) Lacey, S. D.; Kirsch, D. J.; Li, Y.; Morgenstern, J. T.; Zarket, B. C.; Yao, Y.; Dai, J.; Garcia, L. Q.; Liu, B.; Gao, T.; Xu, S.; Raghavan, S. R.; Connell, J. W.; Lin, Y.; Hu, L. Extrusion-Based 3D Printing of Hierarchically Porous Advanced Battery Electrodes. *Adv. Mater.* **2018**, *30*, No. 1705651.
(28) Rojaee, R.; Cavallo, S.; Mogurampelly, S.; Wheatle, B. K.; Yurkiv, V.; Deivanayagam, R.; Foroozan, T.; Rasul, M. G.; Sharifi-Asl, S.; Phakatkar, A. H.; Cheng, M.; Son, S. B.; Pan, Y.; Mashayek, F.; Ganesan, V.; Shahbazian-Yassar, R. Highly-Cyclable Room-Temperature Phosphorene Polymer Electrolyte Composites for Li Metal Batteries. *Adv. Funct. Mater.* **2020**, *30*, No. 1910749.
(29) Biria, S.; Pathreeker, S.; Genier, F. S.; Hosein, I. D. A Highly Conductive and Thermally Stable Ionic Liquid Gel Electrolyte for Calcium-Ion Batteries. *ACS Appl. Polym. Mater.* **2020**, *2*, 2111−2118.
(30) Shim, J.; Lee, J. S.; Lee, J. H.; Kim, H. J.; Lee, J. C. Gel Polymer Electrolytes Containing Anion-Trapping Boron Moieties for Lithium-Ion Battery Applications. *ACS Appl. Mater. Interfaces* **2016**, *8*, 27740−27752.
(31) Wang, C.; Yang, Y.; Liu, X.; Zhong, H.; Xu, H.; Xu, Z.; Shao, H.; Ding, F. Suppression of Lithium Dendrite Formation by Using LAGP-PEO (LiTFSI) Composite Solid Electrolyte and Lithium Metal Anode Modified by PEO (LiTFSI) in All-Solid-State Lithium Batteries. *ACS Appl. Mater. Interfaces* **2017**, *9*, 13694−13702.
(32) Rodrigues, M.-T. F.; Kalaga, K.; Gullapalli, H.; Babu, G.; Reddy, A. L. M.; Ajayan, P. M. Hexagonal Boron Nitride-Based Electrolyte Composite for Li-Ion Battery Operation from Room Temperature to 150 °C. *Adv. Energy Mater.* **2016**, *6*, No. 1600218.
(33) Goodenough, J. B.; Kim, Y. Challenges for Rechargeable Li Batteries. *Chem. Mater.* **2010**, *22*, 587−603.
(34) Cao, D.; Sun, X.; Li, Q.; Natan, A.; Xiang, P.; Zhu, H. Lithium Dendrite in All-Solid-State Batteries: Growth Mechanisms, Suppression Strategies, and Characterizations. *Matter* **2020**, *3*, 57−94.
(35) Gan, H.; Li, S.; Zhang, Y.; Yu, L.; Wang, J.; Xue, Z. Mechanically Strong and Electrochemically Stable Single-Ion Conducting Polymer Electrolytes Constructed from Hydrogen Bonding. *Langmuir* **2021**, *37*, 8270−8280.
(36) Bandhauer, T. M.; Garimella, S.; Fuller, T. F. A Critical Review of Thermal Issues in Lithium-Ion Batteries. *J. Electrochem. Soc.* **2011**, *158*, No. R1.
(37) Zhao, B.; Jiang, L.; Zeng, X.; Zhang, K.; Yuen, M. M. F.; Xu, J.-B.; Fu, X.-Z.; Sun, R.; Wong, C.-P. A Highly Thermally Conductive Electrode for Lithium Ion Batteries. *J. Mater. Chem. A* **2016**, *4*, 14595−14604.
(38) Sharifi-Asl, S.; Lu, J.; Amine, K.; Shahbazian-Yassar, R. Oxygen Release Degradation in Li-Ion Battery Cathode Materials: Mechanisms and Mitigating Approaches. *Adv. Energy Mater.* **2019**, *9*, No. 1900551.
(39) Yin, Y.; Wang, K.; Shen, F.; Han, X. Dendrite-Suppressing Separator with High Thermal Stability Modified by Beaded-Chain-like Polyimide Coating for a Li Metal Anode. *Energy Fuels* **2021**, *35*, 8417−8422.
(40) Deivanayagam, R.; Shahbazian-Yassar, R. Communication—Deconvoluting the Conductivity Enhancement Due to Nanoparticle Fillers in PVdF-Based Polymer Electrolytes for Li-Metal Batteries. *J. Electrochem. Soc.* **2021**, *168*, No. 020525.
(41) Liu, Q.; Cai, B.; Li, S.; Yu, Q.; Lv, F.; Kang, F.; Wang, Q.; Li, B. Long-Cycling and Safe Lithium Metal Batteries Enabled by the Synergetic Strategy of: Ex Situ Anodic Pretreatment and an in-Built Gel Polymer Electrolyte. *J. Mater. Chem. A* **2020**, *8*, 7197−7204.
(42) Tian, H.; Seh, Z. W.; Yan, K.; Fu, Z.; Tang, P.; Lu, Y.; Zhang, R.; Legut, D.; Cui, Y.; Zhang, Q. Theoretical Investigation of 2D Layered Materials as Protective Films for Lithium and Sodium Metal Anodes. *Adv. Energy Mater.* **2017**, *7*, No. 1602528.
(43) Guo, Y.; Qu, X.; Hu, Z.; Zhu, J.; Niu, W.; Liu, X. Highly Elastic and Mechanically Robust Polymer Electrolytes with High Ionic Conductivity and Adhesiveness for High-Performance Lithium Metal Batteries. *J. Mater. Chem. A* **2021**, *9*, 13597−13607.
(44) Falin, A.; Cai, Q.; Santos, E. J. G.; Scullion, D.; Qian, D.; Zhang, R.; Yang, Z.; Huang, S.; Watanabe, K.; Taniguchi, T.; Barnett, M. R.; Chen, Y.; Ruoff, R. S.; Li, L. H. Mechanical Properties of Atomically Thin Boron Nitride and the Role of Interlayer Interactions. *Nat. Commun.* **2017**, *8*, No. 15815.
(45) Xia, Q.; Wu, J.; Shi, Q. X.; Xiang, X.; Li, X.; Pei, H.; Zeng, H.; Xie, X.; Ye, Y. S. UV-Curable Boron Nitride Nanosheet/Ionic Liquid-Based Crosslinked Composite Polymer Electrolyte in Lithium Metal Batteries. *J. Power Sources* **2019**, *414*, 283−292.
(46) Liu, Y.; Qiao, Y.; Zhang, Y.; Yang, Z.; Gao, T.; Kirsch, D.; Liu, B.; Song, J.; Yang, B.; Hu, L. 3D Printed Separator for the Thermal Management of High-Performance Li Metal Anodes. *Energy Storage Mater.* **2018**, *12*, 197−203.
(47) Li, W.; Pang, Y.; Liu, J.; Liu, G.; Wang, Y.; Xia, Y. A PEO-Based Gel Polymer Electrolyte for Lithium Ion Batteries. *RSC Adv.* **2017**, *7*, 23494−23501.
(48) Aldalur, I.; Zhang, H.; Piszcz, M.; Oteo, U.; Rodriguez-Martinez, L. M.; Shanmukaraj, D.; Rojo, T.; Armand, M. Jeffamine Based Polymers as Highly Conductive Polymer Electrolytes and Cathode Binder Materials for Battery Application. *J. Power Sources* **2017**, *347*, 37−46.

https://doi.org/10.1021/acsnanoscienceau.1c00056
ACS Nanosci. Au XXXX, XXX, XXX−XXX